Power System Harmonics Identification Powered by an Eigensystem Realization Approach

Miguel G. Juarez, *Student Member, IEEE*, Felix Reyes-Maldonado, *Student Member, IEEE*, Alejandro Zamora-Mendez, *Member, IEEE*, Jose Ortiz-Bejar, *Member, IEEE*, Juan Carlos Silva-Chavez, *Member, IEEE*, Mario. R. Arrieta Paternina, *Member, IEEE*, and Vicente Torres-Garcia, *Member, IEEE*

***Abstract*—The proliferation of power electronic devices through the massive integration of renewable energy resources in power systems has unleashed high harmonic distortions visible in electrical variables such as voltages and currents. These devices also deteriorate power quality, imposing challenges in quantifying indicators, and advocating novel approaches that deal with this issue. In this context, this paper counteracts such challenges by proposing a strategy to effectively monitor the individual and total harmonic distortions in modern power grids. This proposal exploits a well-known system identification technique, named as the eigensystem realization algorithm, to design a digital filter bank to extract the harmonic components from actual or simulated data. Simulation results of two test systems confirm the effectiveness of the proposed method in attaining reliable estimates for harmonics, inter-harmonics, and sub-harmonics. Furthermore, actual measurements corresponding to the energizing of a bank of three single-phase transformers connected in grounded Wye-Delta are used to demonstrate the proposal in an isolated lab-scale system. The well-known fast Fourier transform (FFT) technique is also applied to validate our proposal, resulting in the proposed ERA-based method is up to 50 times more precise in some cases than FFT.**

Link to graphical and video abstracts, and to code: https://latamt.ieeer9.org/index.php/transactions/article/view/9609

***Index Terms*—Eigensystem realization algorithm, system identification, filter bank frequency response, fast Fourier transform, power quality, total harmonic distortion.**

I. Introduction

In power systems, power quality phenomena are present in the whole grid infrastructure due to the massive integration of distributed energy resources (DERs), the proliferation of non-linear loads, and the massive deployment of power electronics devices. Their presence in the grid has led to increase harmonic pollution, deteriorating the power quality [1], [2].

The associate editor coordinating the review of this manuscript and approving it for publication was Bruno Henrique Groenner Barbosa (*Corresponding author: Alejandro Zamora-Mendez*).

M. G. Juarez, F. Reyes, Alejandro Zamora-Mendez, J. Ortiz, and J. C. Silva are with the Electrical Engineering Faculty, at the Michoacan University of Saint Nicholas of Hidalgo, Morelia, Michoacan, Mexico (e-mail: 1614873c@umich.mx, 1614878b@umich.mx, azamoram@umich.mx, jose.ortiz@umich.mx, and juan.silva@umich.mx).

M. R. A. Paternina is with the Department of Electrical Engineering, National Autonomous University of Mexico, Mexico City 04510, Mexico, (e-mail: mra.paternina@fi-b.unam.mx).

V. Torres is with the TecNM/Instituto Tecnologico de Morelia, Morelia, 58130, Mexico, (e-mail: v.torres@ieee.org).

Harmonics in power systems mean the existence of signals superimposed on the fundamental signal, whose frequencies are integer numbers of the fundamental frequency [3]. Such frequencies cause voltage and current variations from their sinusoidal ideal waveforms, which are evidenced in power quality phenomena, such as reactive power burden and low system efficiency [1], [4]. The presence of supra-harmonics (greater than > 2 kHz) and inter-harmonics has advocated new needs to monitor harmonic distortions in modern electrical systems. For instance, authors in [5] present a compilation of different factors to monitor the harmonic and inter-harmonic pollutions, among the major effects of harmonics, the following are included [3]:

- Capacitor bank failure from dielectric breakdown or reactive power overload.
- Interference with ripple control and power line carrier systems, causing misoperation of systems that accomplish remote switching, load control, and metering.
- Excessive losses in – and heating of – induction and synchronous machines.
- Overvoltages and excessive currents on the system from resonance to harmonic voltages or currents on the network.
- Dielectric breakdown of insulated cables resulting from harmonic overvoltages on the system.
- Inductive interference with telecommunication systems.
- Errors in induction kWh meters.
- Signal interference and relay malfunction, particularly in solid-state and microprocessor-controlled systems.
- Interference with large motor controllers and power plant excitation systems (Reported to cause motor problems as well as non-uniform output.)
- Mechanical oscillations of induction and synchronous machines.
- Unstable operation of firing circuits based on zero-voltage crossing detection or latching.

These effects depend on: the harmonic source, its location, and the network characteristics that promote the propagation of harmonics. Conventionally, the most common method employed to monitor and analyze power system harmonics is the well-known fast Fourier transform (FFT) [2], [6]. For example, in [7], the FFT is used to obtain the magnitude of the fundamental current component and its phase with the non-intrusive load monitoring method for non-intrusive identification of harmonic polluting loads in a smart residential

TABLE I
COMPARISON AMONG DIFFERENT WORKS FOR HARMONICS IDENTIFICATION.

Ref.	Initialization	Prior information	Track freq. variations	Noise immunity
[1], [9]			X	
[10], [11]			X	X
[17]			X	X
[18]	X	X		
[19]	X			X
[20]				X
[21]	X	X	X	
Proposed			X	X

system.

Conversely, different approaches have been proposed in the power system literature, for instance, a survey presented in [8] deepens the state-of-the-art of harmonics and inter-harmonics estimation, exhibiting about 40 methods reviewed and grouped into the following categories: (*i*) parametric/model-based methods, here some methods can be noted as the Prony's analysis [1], [9], the ESPRIT algorithm [10], [11], and the Kalman's filtering algorithm [3]; (*ii*) non-parametric/FFT-based advanced methods as the enhanced fast Fourier transform (e-FFT) [12], where the eFFT model builds up the relationship between inter-harmonic frequency and dispersed leakage energy; (*iii*) statistical techniques such as independent component analysis; (*iv*) machine learning methods as the support vector machine (SVM) algorithm; (*v*) the generalized optimization methods such as the particle swarm optimization (PSO) algorithm; (*vi*) the filter bank (FB)-based methods; and (*vii*) online estimation methods. Alternatively, there are methods to estimate harmonics and inter-harmonics for highly time-varying conditions, among them, the vortex search algorithm (VSA)-based method is presented in [13].

Furthermore, data-driven methods aided by artificial intelligence (AI) have arisen. For instance, an auto-encoder is proposed in [14] to identify waveform distortion caused by photovoltaic installations. A similar study is conducted in [15], where the k-means clustering is fed with features produced by an auto-encoder to determine equipment causing harmonic distortions. To see more AI applications, a comprehensive survey in harmonic analysis is found in [16].

Comparisons of different parametric/model-based methods used for harmonic identification are summarized in Table I, where features are employed to contrast them in terms of: requirements about initialization and prior information, their capabilities to track frequency variations, and their noise immunit. Notice that our proposal exhibits similar features that ESPRIT and matrix pencil methods. In this context, our contribution lies in estimating power system harmonics, inter-harmonics, and sub-harmonics using the eigenvalue identification method to capture harmonic features from measurement or simulated data. The proposed method extends the state-of-the-art of parametric/model-based methods by introducing the eigensystem realization algorithm (ERA).

A. Contribution

The novelty of this investigation lies in the power system harmonic identification powered by the ERA method. This approach consists of a system identification technique that allows us to design a filter bank for extracting harmonic components from actual or simulated data, being more flexible and adaptable than the Fourier filters which take into account only a fixed frequency. The ERA filter bank is also able to provide damping and frequency estimates, giving more useful information than Fourier. Thus, the primary contributions of this paper are summarized as follows:

- The estimation achieved by the ERA method allows us to correctly extract harmonics, inter-harmonics, and sub-harmonics from actual or simulated data.
- The proposed method extends the state-of-the-art of parametric/model-based methods by introducing the ERA technique.
- The proposed method adopts a dynamic model to capture harmonic patterns instead of a static paradigm.
- A powerful tool for processing harmonic estimations based on a set of ERA-based FIR filters is proposed to power system community.

II. FUNDAMENTALS

This section briefly describes the ERA method for a single channel to monitor harmonic components by taking advantage of the ERA-based FIR filter design and its ability to perform frequency identification and frequency tracking.

A. Eigensystem Realization Algorithm

This technique is a modal identification algorithm that involves the system realization theory for the construction of state-space models ($[\mathbf{A}, \mathbf{B}, \mathbf{C}, \mathbf{D}]$) of linear systems.

The ERA is based on the singular value decomposition (SVD) of the Hankel matrix $\mathbf{H}_0$ associated with the time response of a linear system [22], [23]. A pseudo-code for the single-channel ERA method is detailed in **Algorithm 1**, where the Hankel matrices $\mathbf{H}_0$ and the shifted $\mathbf{H}_1$ are assembled employing the complete data of recorded signal such that the top left-most element of $\mathbf{H}_0$ is $s(0)$ and the bottom right-most element of $\mathbf{H}_1$ is $s(N)$ with N samples ($k = 0, \ldots, N$) until complete 12-cycles for a sample frequency [22]. It is important to mention that the ERA can work like a filter bank with the ability to capture harmonic patterns contained in a multi-modal signal, such as frequency, amplitude, and phase, as can be seen in (7) and (8), respectively. Furthermore, with these features, the individual and total harmonic distortions can be computed by (9), whereas the reconstruction signal can be computed with (10). Thus, the ERA-based filter can perform harmonics monitoring in power systems, thanks to Vandermode's pseudoinverse matrix, which contains a set of FIR filters that enable the extraction of harmonic features. This can be seen in (6) in **Algorithm 1** and described in the following section.

Algorithm 1 ERA for harmonic identification.

1: **Input:** A time-series data of recorded signal $s(k)$ of $N = 12$ cycles length.
2: **Outputs:** Harmonic parameters: f_h, A_h, ϕ_h, THD, and $\hat{s}(k)$.
3: To assemble the Hankel matrices $\mathbf{H}_0$ and the shifted $\mathbf{H}_1$ by means of the signal samples data
4: To apply SVD to the Hankel matrix $\mathbf{H}_0$ for obtaining a system with h terms (harmonics): ▷

$$\mathbf{H}_0 = \mathbf{U}\boldsymbol{\Sigma}\mathbf{V}^T = \begin{bmatrix}\mathbf{U}_h & \mathbf{U}_s\end{bmatrix}\begin{bmatrix}\boldsymbol{\Sigma}_h & 0\\ 0 & \boldsymbol{\Sigma}_s\end{bmatrix}\begin{bmatrix}\mathbf{V}_h^T\\ \mathbf{V}_s^T\end{bmatrix} \tag{1}$$

5: To approximate the high-rank Hankel matrix $\mathbf{H}_0$ by a reduced-rank h matrix: ▷

$$\mathbf{H}_0 \approx \mathbf{U}_h\boldsymbol{\Sigma}_h\mathbf{V}_h^T \tag{2}$$

6: To compute matrix $\mathbf{A}$: ▷

$$\mathbf{A} = \boldsymbol{\Sigma}_h^{-\frac{1}{2}}\mathbf{U}_h\mathbf{H}_1\mathbf{V}_h^T\boldsymbol{\Sigma}_h^{-\frac{1}{2}} \tag{3}$$

7: To compute eigenvalues in discrete and continuous time at each harmonic frequency: $z_h = eig(\mathbf{A})$ ▷

$$\lambda_h = \frac{\ln(z_h)}{\Delta t} \tag{4}$$

8: To find the h-th residues B from:

$$\begin{bmatrix} z_1^{-N/2} & z_2^{-N/2} & \cdots & z_n^{-N/2}\\ \vdots & \vdots & \ddots & \vdots\\ z_1^0 & z_2^0 & \cdots & z_n^0\\ \vdots & \vdots & \ddots & \vdots\\ z_1^{N/2} & z_2^{N/2} & \cdots & z_n^{N/2}\end{bmatrix}\begin{bmatrix}B_{N/2}\\ \vdots\\ B_0\\ \vdots\\ \bar{B}_{N/2}\end{bmatrix} = \begin{bmatrix}y(0)\\ y(1)\\ \vdots\\ y(N)\end{bmatrix} \tag{5}$$

▷ where matrix $\mathbf{Z}$ is a Vandermode matrix.
9: To obtain the impulse responses of the ERA-based filters from the rows of the Moore-Penrose pseudoinverse:

$$\mathbf{Z}^\dagger = (Z^H Z)^{-1} Z^H \tag{6}$$

10: To compute harmonic frequencies:

$$\hat{f}_h = \mathrm{Im}\left(\frac{\lambda_h}{2\pi}\right) \tag{7}$$

11: TO compute harmonic amplitudes and phases from the h-th residues:

$$A_h = 2|B_h|; \qquad \phi_h = \angle B_h \tag{8}$$

12: To compute IHD and THD:

$$\begin{aligned}\%IHD &= \frac{V_{h,RMS}}{V_{1,RMS}} \times 100 \quad \forall h = 2,\ldots,H;\\ \%THD &= \frac{\sqrt{\sum_{h=2}^{H} V_{h,RMS}^2}}{V_{1,RMS}} \times 100\end{aligned} \tag{9}$$

13: To perform the signal reconstruction:

$$\hat{s}(k) = \sum_{h=1}^{H} A_h \cos\left(2\pi f_h k + \phi_h\right) \tag{10}$$

B. Frequency Response of the ERA-Based FIR Filters

The rows of the Moore-Penrose pseudoinverse matrix in (6) are the reflected impulse responses of the ERA-based filters, where the H in (6) stands for the Hermitian operator of the complex matrix $\mathbf{Z}$, whereas the H in (9) and (10) indicates the number of harmonics $h = 1, 2, \ldots, H$. Thus, the frequency responses of the impulse responses can be obtained using the FFT and ERA-based approaches, as shown in plots (a)-(b) of Fig. 1. For the ERA-based filter bank, r=1 and N = 16 samples are assumed in (11), where the complex matrix $\mathbf{Z}$ is constructed as follows:

$$\mathbf{Z} = \begin{bmatrix} (re^{\frac{i\pi}{N}})^{-N/2} & \ldots & (re^{\frac{i4\pi}{N}})^{-N/2} & (re^{\frac{i2\pi}{N}})^{-N/2} & 1 & (re^{\frac{-i2\pi}{N}})^{-N/2} & (re^{\frac{-i4\pi}{N}})^{-N/2} & \ldots & (re^{\frac{-i\pi\pi}{N}})^{-N/2}\\ \vdots & \vdots & \vdots & \vdots & 1 & \vdots & \vdots & \vdots & \vdots\\ (re^{\frac{i\pi\pi}{N}})^{-2} & \ldots & (re^{\frac{i4\pi}{N}})^{-2} & (re^{\frac{i2\pi}{N}})^{-2} & 1 & (re^{\frac{-i2\pi}{N}})^{-2} & (re^{\frac{-i4\pi}{N}})^{-2} & \ldots & (re^{\frac{-i\pi\pi}{N}})^{-2}\\ (re^{\frac{i\pi\pi}{N}})^{-1} & \ldots & (re^{\frac{i4\pi}{N}})^{-1} & (re^{\frac{i2\pi}{N}})^{-1} & 1 & (re^{\frac{-i2\pi}{N}})^{-1} & (re^{\frac{-i4\pi}{N}})^{-1} & \ldots & (re^{\frac{-i\pi\pi}{N}})^{-1}\\ 1 & \ldots & 1 & 1 & 1 & 1 & 1 & \ldots & 1\\ (re^{\frac{i\pi\pi}{N}})^{1} & \ldots & (re^{\frac{i4\pi}{N}})^{1} & (re^{\frac{i2\pi}{N}})^{1} & 1 & (re^{\frac{-i2\pi}{N}})^{1} & (re^{\frac{-i4\pi}{N}})^{1} & \ldots & (re^{\frac{-i\pi\pi}{N}})^{1}\\ (re^{\frac{i\pi\pi}{N}})^{2} & \ldots & (re^{\frac{i4\pi}{N}})^{2} & (re^{\frac{i2\pi}{N}})^{2} & 1 & (re^{\frac{-i2\pi}{N}})^{2} & (re^{\frac{-i4\pi}{N}})^{2} & \ldots & (re^{\frac{-i\pi\pi}{N}})^{2}\\ \vdots & \vdots & \vdots & \vdots & 1 & \vdots & \vdots & \vdots & \vdots\\ (re^{\frac{i\pi\pi}{N}})^{N/2} & \ldots & (re^{\frac{i4\pi}{N}})^{N/2} & (re^{\frac{i2\pi}{N}})^{N/2} & 1 & (re^{\frac{-i2\pi}{N}})^{N/2} & (re^{\frac{-i4\pi}{N}})^{N/2} & \ldots & (re^{\frac{-i\pi\pi}{N}})^{N/2}\end{bmatrix} \tag{11}$$

As can be noted in Fig. 1, the frequency response of the ERA-based filter bank looks similar to those filters provided by the FFT. The main advantage of our proposal is the provision of new features such as its adaptive ability to perform frequency identification without any prior knowledge and to track frequency variations, both are helpful to monitor harmonics in power systems. Fig. 2 briefly summarizes the methodology, showing that a 12-cycle signal of the fundamental frequency is required as input. The ERA-based FIR filter bank is then applied to determine the harmonic frequencies, amplitudes, and phase angles. The signal is then reconstructed and compared with the original signal to calculate the reconstruction error and validate the proposal.

Fig. 3 also shows the block diagram of a conventional power quality analyzer in which this methodology could be implemented, replacing the FFT filters commonly used by commercial analyzers with the ERA filters or implementing a prototype developed in a micro-controllers or digital signal processors, resulting in a low-cost and small-sized meter.

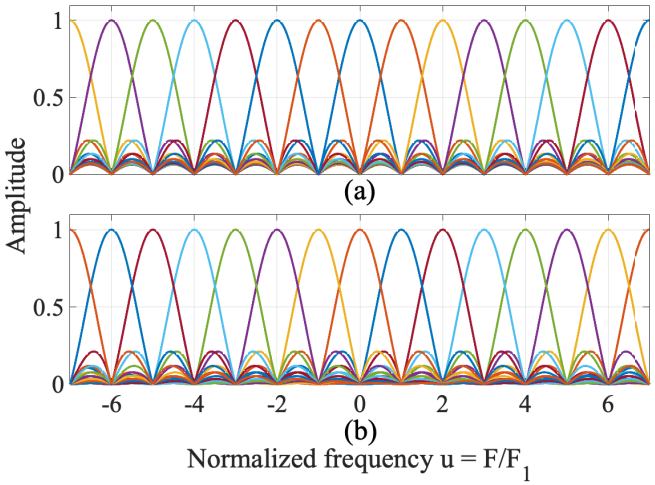

Fig. 1. Filter bank's frequency responses of: (a) FFT and (b) ERA-based method.

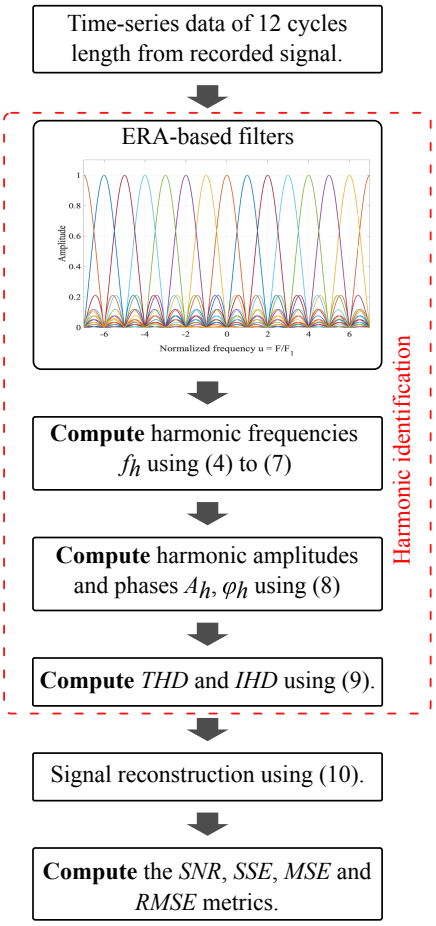

Fig. 2. ERA filter bank flowchart for harmonic identification.

C. Eigensystem Realization for Harmonic Estimation Assessment

To evaluate the performance of the ERA-based FIR filter bank for harmonic monitoring, a periodic synthetic signal at the fundamental frequency with dynamic phase passed through a nonlinear device is used as follows [24]:

$$s(t) = \tanh\left(3x(t)\right) \tag{12}$$

where

$$x(t) = \cos\left(2\pi t + \varphi(t)\right), \tag{13}$$

and

$$\varphi(t) = 1 - e^{-t/10}\cos\left(2\pi t/5\right) \tag{14}$$

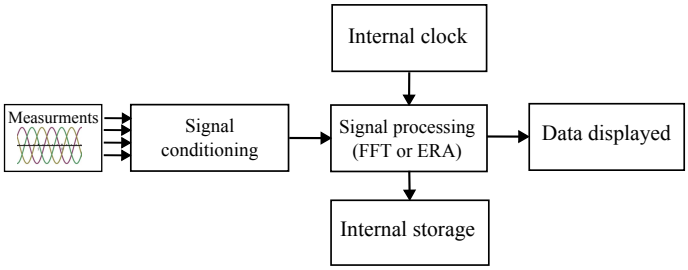

Fig. 3. Block diagram of the stages that make up a conventional power quality analyzer.

This synthetic signal is sampled at N= 128 samples per fundamental cycle and contains 3rd, 5th, 7th, and 9th harmonics [24]. According to the IEC standard [25], a 10-cycle signal segment at 50 Hz fundamental frequency or a 12-cycle signal segment at 60 Hz fundamental frequency must be used for harmonic distortion analysis. Thus, this paper adopts a 60 Hz fundamental frequency with a 12-cycle analysis for all cases.

The synthetic signal in Fig. 4(a) is processed through the ERA-based spectra using (6) and is compared with the Fourier's spectrum. It is notorious the similitude among Figs. 4(b)-(c), since both frequency responses match specifically in the first five odd-harmonic components (1st, 3rd, 5th, 7th, and 9th).

After assessing the frequency domain, we proceed to evaluate the ability of the ERA-based filter to perform harmonic analysis and how its estimates can reconstruct the synthetic signal. This fact can be observed in Fig. 5, where the signal reconstruction in (10) exhibits that both methods properly synthesize the actual signal (continuous line). Figure 6 illustrates the harmonic segregation of the theoretical signal using the proposed ERA-based filter and its comparison with the FFT. To quantify the approximation error, the proposed method and the FFT are contrasted against the actual signal by computing the following metrics [26]: signal-to-noise ratio (SNR), sum of squared errors (SSE), mean squared error (MSE), and root-mean-square error (RMSE). For example, the SNR error is given by [27]:

$$SNR = 10\log_{10}\left(\frac{s^2}{s^2 - \hat{s}^2}\right) \tag{15}$$

where s is the actual signal to be analyzed, and $\hat{s}$ is the reconstruction signal by means of (10) and all harmonic parameters estimates for each method. The results after quantifying these metrics are summarized in Table II.

Thanks to the ability to track changes in frequency and phase, the ERA-based filter showcases a better performance for all metrics in comparison with the FFT, where the ERA approach has a minor error in the harmonic estimation with 105.6708 times smaller than FFT.

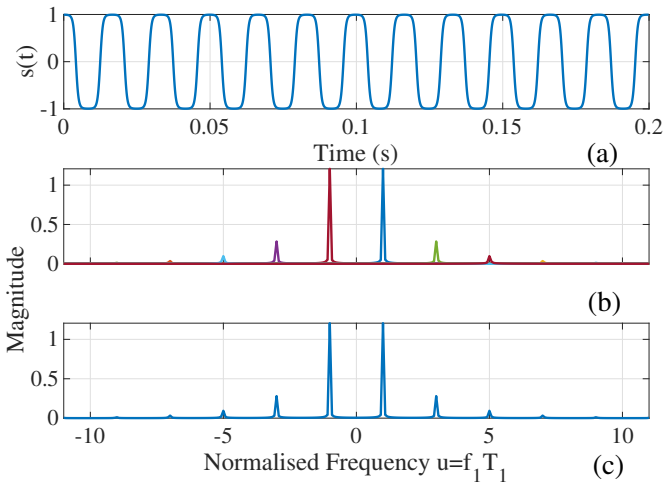

Fig. 4. Theoretical waveform including harmonics and its spectra. (a) Signal. (b) ERA-based spectrum. (c) Fourier spectrum.

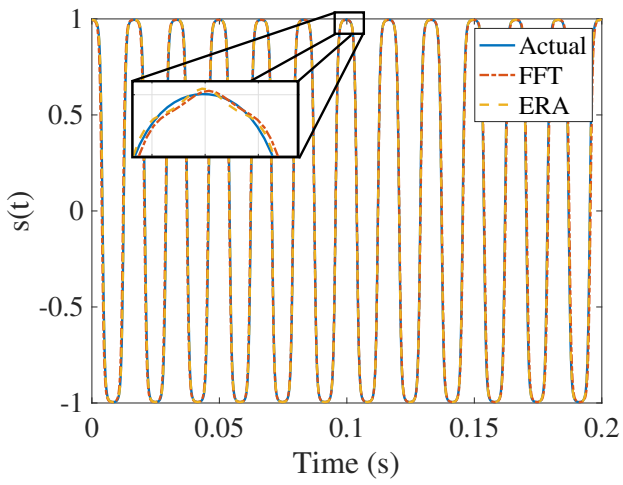

Fig. 5. Performance in reconstructing an actual signal through the harmonic estimates of the FFT and ERA-based methods.

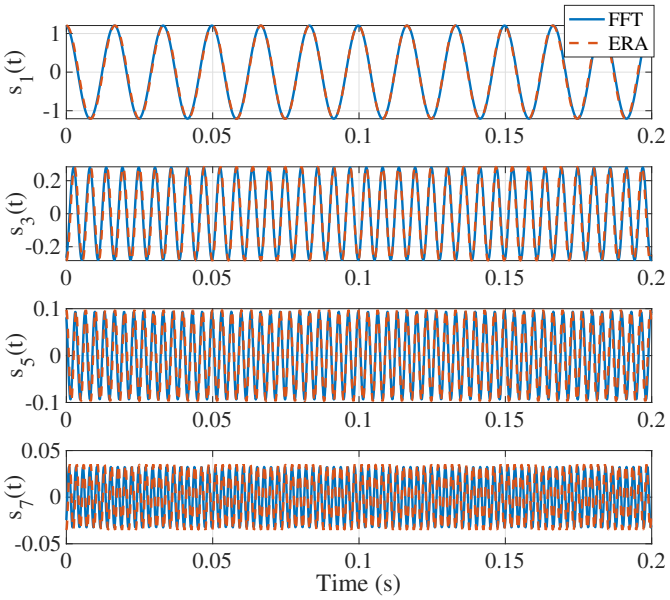

Fig. 6. Harmonic decomposition of $s(t)$ using FFT and ERA-based methods.

Furthermore, Table III compares harmonic frequencies and amplitudes obtained using the ERA method in (7) and compared with the FFT in (8). Notice the numeric precision of our proposal for both features in the first 6 odd harmonics.

Details about the computational complexity are found in Section 3.1 of ref. [28]. For harmonic analysis, the computational burden mainly is integrated by: the SVD computation of the Hankel matrix in (1), the eigenvalues' computation of matrix $\mathbf{A}$ in (3), and the Moore-Penrose pseudoinverse's computation in (6). For this case study, the SVD of matrix $\mathbf{H}_0 \in \mathbb{R}^{767\times767}$ implies $4m^2n+8mn^2+9n^3$ operations, resulting in a total of 9.4756 $\times10^9$. Since matrix $\mathbf{A}$ in (3) is $\mathbb{R}^{14\times14}$, the eigenvalues' computation implies 14^3 multiplications due to its cubic complexity [28]. Matrix $\mathbf{Z}^\dagger \in \mathbb{R}^{1537\times14}$ then requires 1537^14 products. Thus, the total computational burden defined in terms of the number of operations becomes 9.4779 $\times10^9$. By implementing the proposal on a microprocessor with 0.83 ns of instruction cycle time, such as a PowerPC 970 MP RISC, then the total computation time becomes 7.8667 s [29].

TABLE II
RESULTS AFTER QUANTIFYING THE ERA-BASED FILTER AND FFT

Error	**ERA-based filter**	**FFT**
SNR	47.2006 dB	22.4469 dB
SSE	0.0006 A^2	6.7790 A^2
MSE	0.0000 A^2	0.0044 A^2
$RMSE$	0.0006 A	0.0664 A

TABLE III
COMPARISON OF HARMONIC FREQUENCIES AND AMPLITUDES PROCESSED BY THE ERA-BASED APPROACH AND FFT ANALYSIS FOR HARMONIC ESTIMATION OF THE THEORETICAL SIGNAL

Harm. order	Frequency (Hz)		Amplitude (pu)	
	FFT	ERA	FFT	ERA
1	60	60.1651	1.2056	1.2074
3	180	180.4954	0.2800	0.2840
5	300	300.8256	0.0936	0.0975
7	420	421.1559	0.0325	0.0352
9	540	541.4860	0.0112	0.0129
11	660	661.8156	0.0038	0.0047
13	780	782.1416	0.0013	0.0017

III. TEST CASES AND RESULTS

This section confirms the effectiveness of the ERA-based FIR filter bank to monitor harmonics in active power grids. To this end, the proposal's performance is assessed through three case studies consisting of: (*i*) harmonic analysis of an uncontrolled three-phase rectifier; (*ii*) a modified-Kundur two-area power system including a wind power plant (WPP) equipped with a Type-3 wind turbine generator (WTG); and (*iii*) a real transient event captured by a power quality analyzer. The first two cases are implemented using Matlab & Simulink platforms, and the latter is a transient event captured from a laboratory implementation. They are described in detail in the following.

A. Harmonic Analysis of an Uncontrolled Three-Phase Rectifier

This test comprises the harmonic analysis of an uncontrolled three-phase rectifier [30], as illustrated in Fig. 7. The test system has the following parameters: (*i*)rated AC voltage, $V_{Rated} = 4160$ V at 60 Hz, (*ii*) AC real power load, $P_{AC} = 5$ MW, and (*iii*) DC real power load, $P_{DC} = 5$ MW.

For the testing circuit, the AC load is set to consume 5 MW, whereas the DC load consumes approximately 5 MW, and the currents' waveforms are exhibited in Fig. 8. The harmonic analysis is conducted using a sampling rate of 10 kHz and a 12-cycle analysis window of the fundamental frequency, as a commercial power quality analyzer does [31].

By using the ERA-based method in **Algorithm 1**, the harmonic monitoring is carried out processing current in phase

a in Fig. 8 that results in a high harmonic distortion, as depicted in Fig. 9. Notice the presence of odd harmonics, where the h-th harmonic in the order of 5, 7, 11, 13, 17, 19, 23, 25, and 29 are identified. For comparison purposes, an FFT analysis is also applied to the same waveform, achieving high similitude results to those attained by the ERA-based technique. The total harmonic distortion in the current (THD_i) is computed by using (9) and compared with the one obtained by the FFT method, where the ERA-based method quantifies a 14.17%, instead of a 13.36% as Fourier does.

Besides, the frequency response of the ERA-based filters obtained with (6) is depicted in Fig. 10(a), where the filters extract the fundamental component and its harmonics. Conversely, Fig. 10(b) shows the same filters, but now they are obtained with the well-known FFT method. Notice the similitude in both frequency responses.

Table IV summarizes the details of harmonic order, fundamental frequency by (7), and harmonic amplitude using (8), derived by the ERA-based approach and compared with FFT analysis. These results are employed to corroborate the estimates obtained with the proposed method.

TABLE IV
RESULTS OF HARMONIC MONITORING VIA THE ERA-BASED AND FFT ANALYSES FOR AN UNCONTROLLED THREE-PHASE RECTIFIER

Harm. order	Frequency (Hz)		Amplitude (A)		Phase (degrees)	
	FFT	ERA	FFT	ERA	FFT	ERA
1	60.00	60.00	1945.8057	1945.8057	92.7138	88.3933
5	300.00	300.00	218.86	218.8588	-82.0654	-103.6319
7	420.00	420.00	105.84	105.8404	-84.1462	-114.3366
11	660.00	660.00	85.132	85.1301	104.5927	57.1234
13	780.00	780.00	57.595	57.5929	103.3049	47.2477
17	1020.00	1020.00	50.421	50.4306	-68.7644	-142.1397
19	1140.00	1140.00	37.616	37.6279	-68.8404	-150.8458
23	1380.00	1380.00	33.854	33.8516	118.1564	18.7977
25	1500.00	1500.00	26.502	26.4998	119.4237	11.4834
29	1740.00	1740.00	23.984	23.9981	-54.9028	-179.8383

Thanks to the reconstruction capacity of the proposed approach and the Fourier analysis, time-frequency comparisons can be established by using the reconstructed signals in Fig. 11, where it can be recognized that the approximation of the ERA-based technique provides the lowest error. The reconstruction's errors in Table V are quantified for both methods, using the following metrics: SNR, SSE, MSE, and RMSE.

Notice that the proposal's harmonic estimates have the lowest error. The SNR in (15) becomes 34.53 dB for ERA-based harmonic estimation. This value indicates an error between

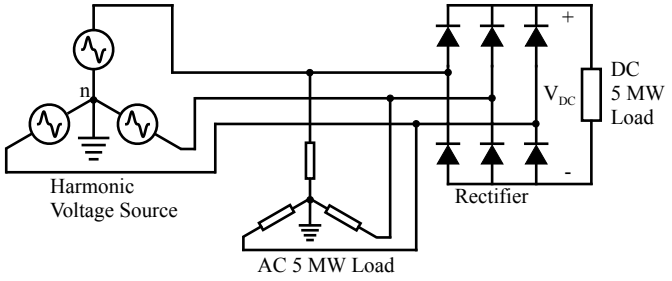

Fig. 7. Three-phase AC system equipped with harmonic voltage source, AC load, an uncontrolled three-phase rectifier, and DC load.

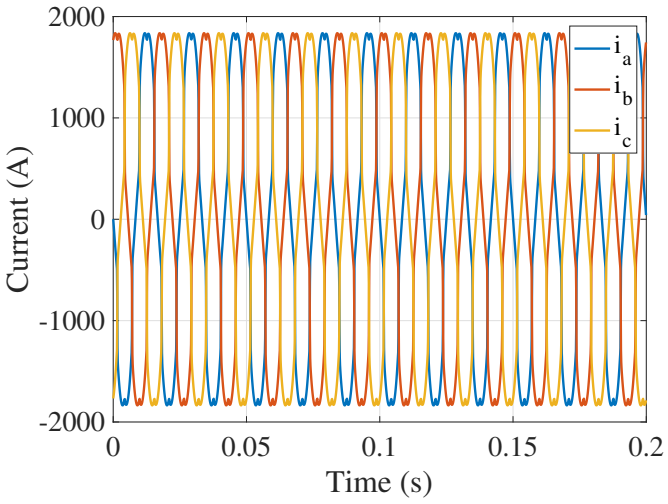

Fig. 8. Currents' waveforms of the uncontrolled three-phase rectifier.

TABLE V
SNR, SSE, MSE, AND RMSE ERRORS FOR AN UNCONTROLLED THREE-PHASE RECTIFIER

Error	**ERA-based filter**	**FFT**
SNR	34.5300 dB	33.9767 dB
SSE	1,547,025.6152 A^2	1,546,067.9298 A^2
MSE	771.9688 A^2	773.4206 A^2
$RMSE$	27.7843 A	27.8104 A

reconstructed and actual signals, reaching up to 3.4 times smaller than that obtained with the FFT approach, achieving a suitable matching by the ERA approach. These metrics corroborate that the THD obtained by the ERA-based approach represents a better approximation. Moreover, Fig. 12 shows the reconstruction error for the ERA and FFT filters, where it can be recognized that the approximation of the ERA filter bank provides the lowest error.

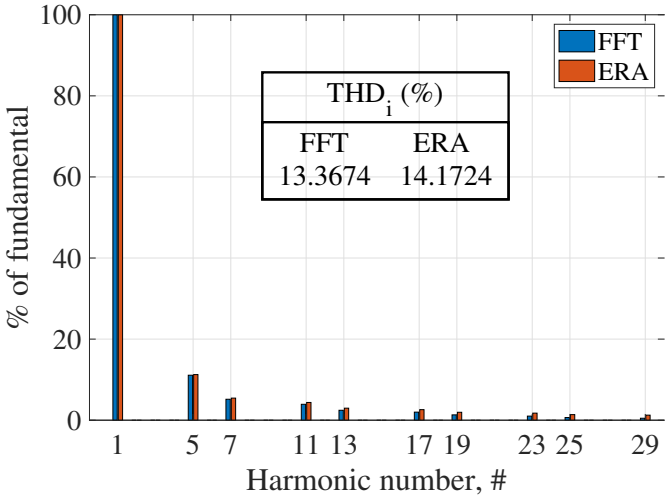

Fig. 9. Comparing results of individual and total harmonic monitoring in a current waveform between the ERA-based proposal and Fourier analysis.

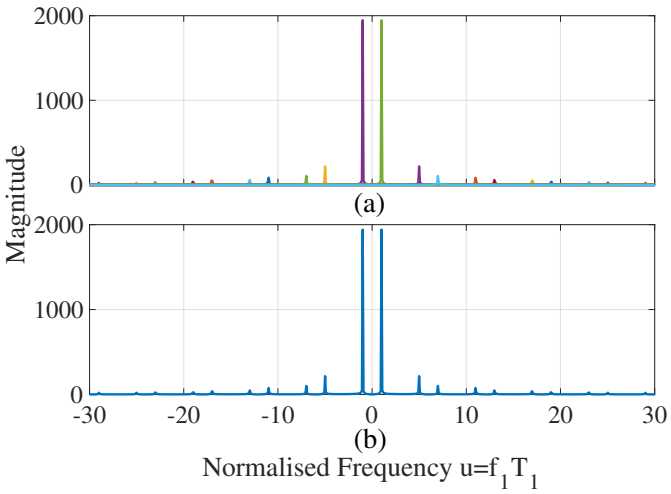

Fig. 10. Filter's frequency responses for performing harmonic analysis: (a) ERA-based filters, and (b) FFT filters.

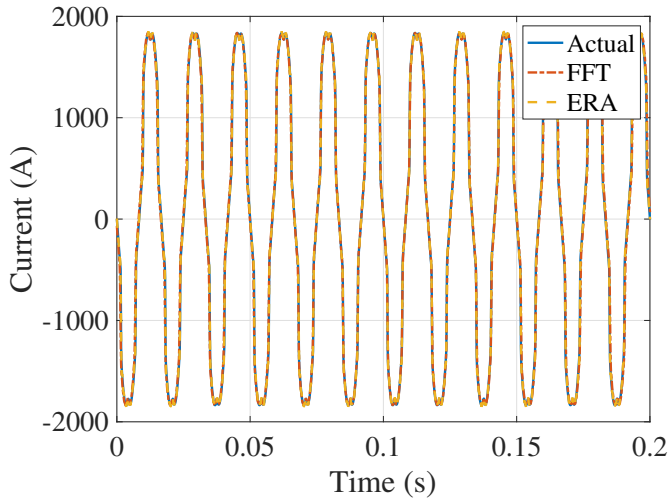

Fig. 11. Reconstruction capacity of a current waveform through the FFT and ERA-based analyses.

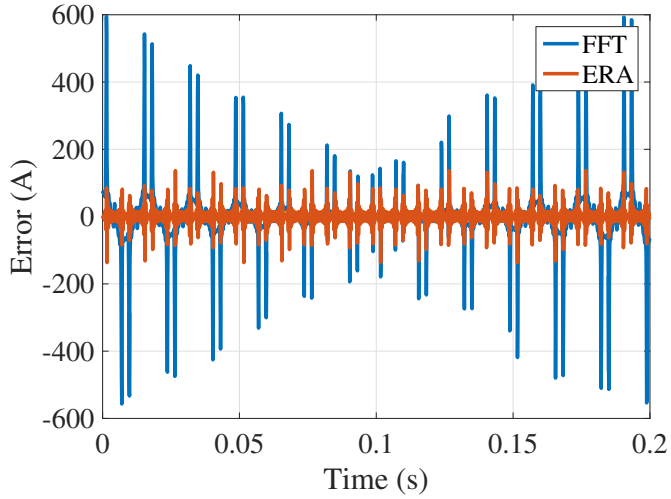

Fig. 12. Reconstruction errors of the FFT and ERA-based analyses for the current waveform of the uncontrolled three-phase rectifier.

B. Modified Kundur Two-Area Power System

This case deals with harmonic monitoring in a well-known power grid as Kundur's system [32]. To carry out this analysis, the system is modified incorporating a wind power plant (WPP) and modeled in Matlab & Simulink, as can be seen in Fig. 13(a), whose one-line diagram is exhibited in Fig. 13(b). It contains 4 synchronous generators (SGs) with a rating power of 900 MVA and 20 KV at 60 Hz, 11 buses, and two areas interconnected by a tie-line. All SGs are modeled using a 4-th order generator model and static excitation systems. The WPP is considered to have 20 MVA and consists of two 10 MVA Type-3 WTGs. Thus, the WPP is emulated as a three-phase harmonic voltage injection into bus 8, so that low-order odd harmonics (5-th, 7-th, 11-th) due to harmonic currents in Type-3 WTGs can be introduced to the power system [33]. Additionally, an inter-harmonic of 5.5 times the fundamental frequency is mainly produced by the rapid non-periodic changes in current and voltage caused by: loads operating in a transient state (temporarily or permanently) or when voltage modulation is implemented or current amplitude for control purposes. These changes can be random, or depending on the process and controls used [34]. Additionally, a sub-harmonic of 0.45 times the fundamental frequency is also generated by the WPP [35], [36]. All harmonic components are considered to be 0.1 pu, thus they can be present for voltage and current signals in the system [33].

For this case study, voltage and current measurements in phase a (v_a and i_a) at bus 2 of Fig. 13(a) are analysed by using the proposed method for harmonic monitoring. The sampling rate for this test system is 7680 Hz with a 12-cycle analysis window at 60 Hz. Both signals are illustrated in Fig. 14.

The harmonic analysis of voltage and current waveforms collected at bus 2 is performed by the ERA-based method and compared with the FFT analysis, as shown in Fig. 15. Notice that the harmonic analysis for the voltage signal is shown in plot (a) and for the current signal in plot (b). For both voltage and current signals, the attained results by the ERA method are very similar to those obtained by the FFT, where the voltage THD (THD_v) is 7.61% and 7.55% for ERA and Fourier, respectively. For the current signal, the current THD (THD_i are 5.53% and 5.74% for the ERA and FFT approaches, respectively.

The frequency responses of the ERA and FFT filters for the voltage signal are illustrated in Fig. 16(a)-(b), respectively, where the filters to extract the mono-components of the voltage signal can be observed. Similarly, Figures 17(a)-(b) show the frequency responses of both methods for the current signal.

All details about the harmonic monitoring employing the ERA and FFT methods applied to both voltage and current signals at bus 2 are depicted in Tables VI and VII, respectively. These results corroborate the estimates obtained with the proposed method, where the reconstructed signals are displayed in Fig. 18, exhibiting a high match. Notice that for the sub-harmonic, its actual frequency is at 27 Hz, the ERA method can identify this frequency very well, whereas the FFT identifies this frequency at 25 Hz.

By following our methodology, error metrics such as the

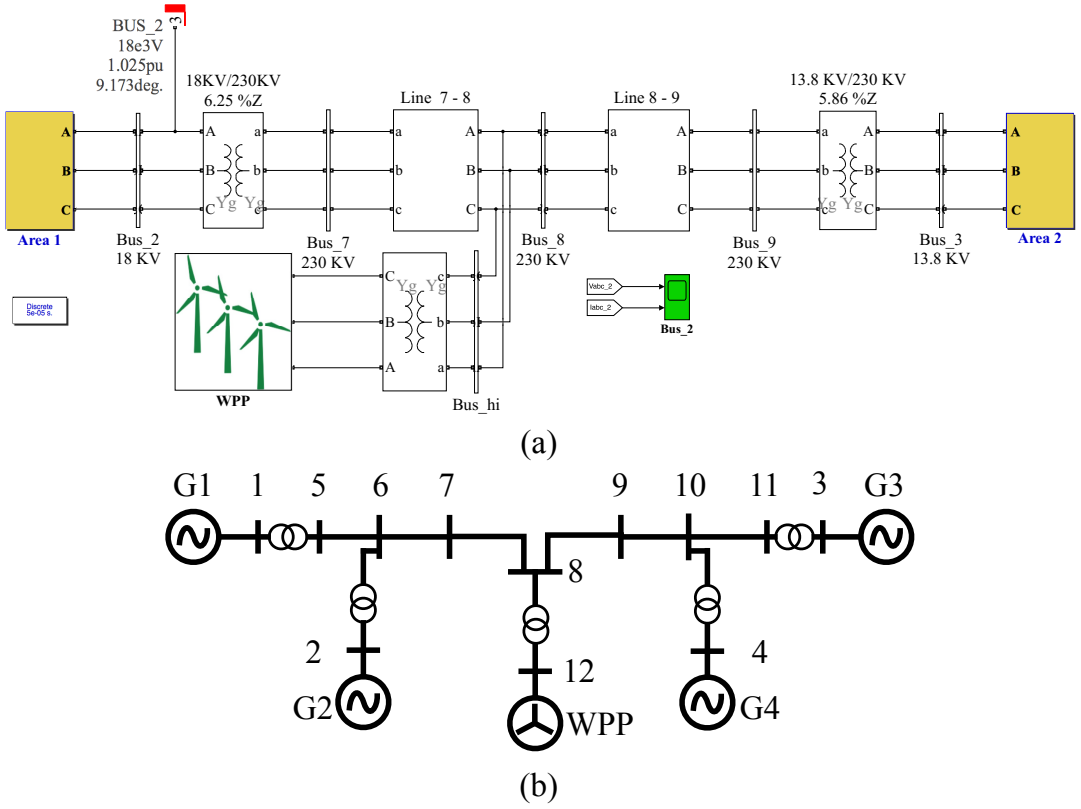

Fig. 13. Kundur power system with a wind power plant. (a) Simulink model, and (b) single line diagram.

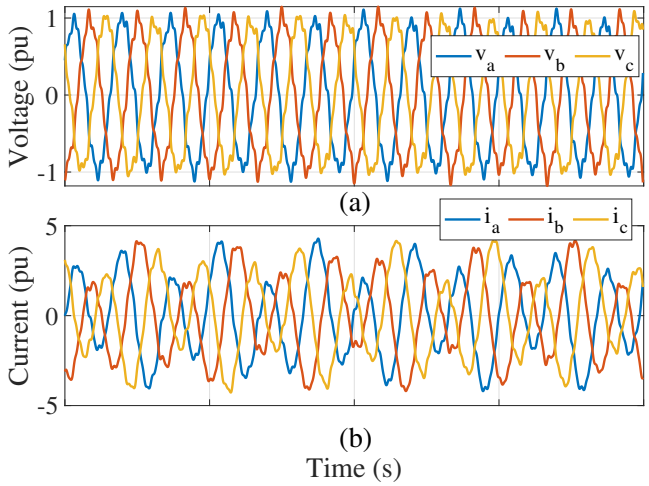

Fig. 14. Voltage and current signals at bus 2 of the Kundur power system.

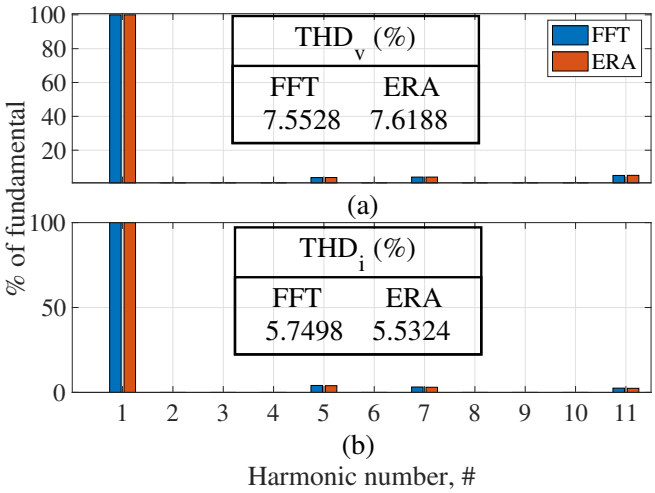

Fig. 15. Individual and total Harmonic analyses in the Kundur power system through the proposal and Fourier approaches. Processing in: (a) voltage signal at bus 2, and (b) for current signal.

SNR, SSE, MSE, and RMSE quantify the reconstruction capacity. The voltage and current signals of the Kundur system in both methods are summarized in Tables VIII and IX, respectively.

Even though the FFT and ERA-based filters are very similar, it is notorious that our proposal has the lowest error, being 12.8 and 52.7 times smaller than FFT for voltage and current, respectively, as indicated in all error metrics. This means that filters in Figs. 16 and 17 correctly identify and extract the harmonic components. Furthermore, the reconstruction errors are displayed in Fig. 19 for the ERA and FFT methods, where it can be noticed that the best approximation is provided by ERA, despite the filter bank closely resembling those obtained through the FFT filters.

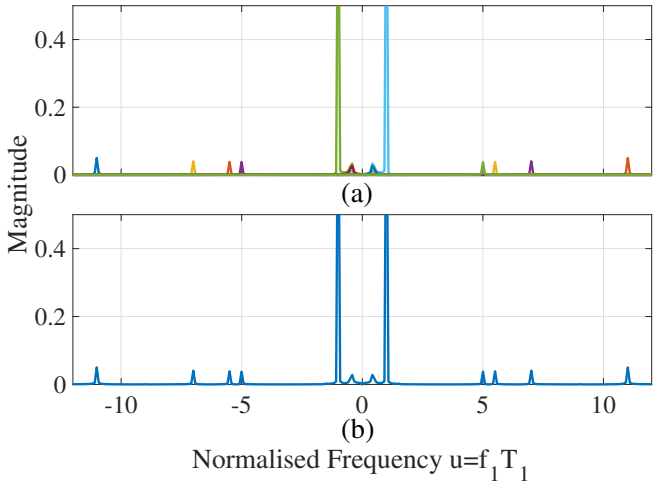

Fig. 16. Frequency responses for the voltage signal at bus 2 of the Kundur power system. (a) ERA filters and (b) FFT filters.

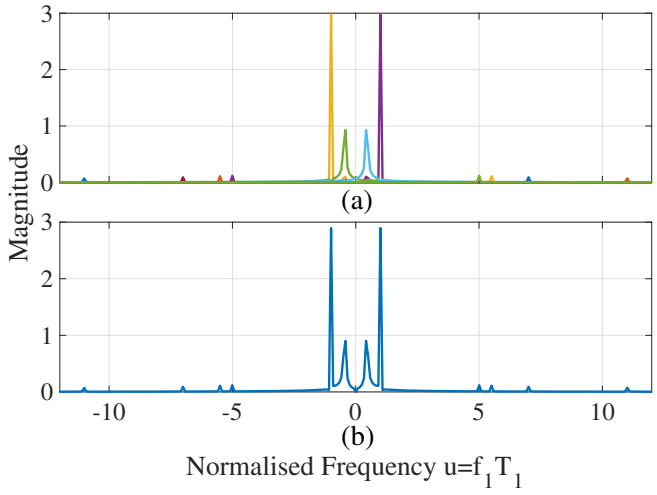

Fig. 17. Frequency responses of the current signal at bus 2 of the Kundur power system processed by: (a) ERA filters, and (b) FFT filters.

TABLE VI
RESULTS OF HARMONIC MONITORING THROUGH THE ERA-BASED AND FOURIER APPROACHES OF THE VOLTAGE SIGNAL AT BUS 2 OF THE KUNDUR SYSTEM

Harm. order	Frequency (Hz) FFT	Frequency (Hz) ERA	Amplitude (pu) FFT	Amplitude (pu) ERA	Phase (degrees) FFT	Phase (degrees) ERA
0.45	25	26.9971	0.0272	0.0352	-155.1548	133.1378
1	60	60.0004	0.9886	0.9891	-70.4958	-71.5214
5	300	299.9986	0.0380	0.0381	-81.2547	-85.9721
5.5	330	329.9988	0.0381	0.0386	-79.9034	-85.0925
7	420	419.9992	0.0403	0.0407	-77.5715	-84.1631
11	660	659.9997	0.0500	0.0505	-73.7717	-84.0987

C. Real transient event application

The energizing of a three-phase transformer in an isolated lab-scale system is carried out for this case. The current signal in phase a is captured once the inrush current transient is over, provoking a distortion in the current waveform to be used for the harmonics analysis. The lab-scale system consists of three identical single-phase transformer units (3 kVA, 220V) to form a grounded Wye-Delta three-phase transformer connection, which is connected to a three-phase voltage source ($V_L = 220$ V). To record the transient event, a commercial power quality analyzer is connected at the primary side, whereas the secondary side is left open, measuring voltages and currents instantaneously [31]. Fig. 20 displays the current waveform captured by the PQ analyzer that is featured by a 12-cycle duration and a sampling rate of 12.5 kHz.

Fig. 21 depicts the harmonic analysis of the current wave-

TABLE VII
RESULTS OF HARMONIC MONITORING THROUGH THE ERA-BASED AND FOURIER APPROACHES OF THE CURRENT SIGNAL AT BUS 2 OF THE KUNDUR SYSTEM

Harm. order	Frequency (Hz) FFT	Frequency (Hz) ERA	Amplitude (pu) FFT	Amplitude (pu) ERA	Phase (degrees) FFT	Phase (degrees) ERA
0.45	25	26.9996	0.8964	1.2165	-63.5912	-137.6838
1	60	59.9988	2.9000	2.9712	-82.6942	-83.4742
5	300	300.0048	0.1191	0.1179	12.5518	1.9901
5.5	330	330.0045	0.1091	0.1091	12.5852	1.6226
7	420	420.0039	0.0904	0.0905	13.1711	1.1311
11	660	660.0026	0.0711	0.0718	12.1574	-2.5528

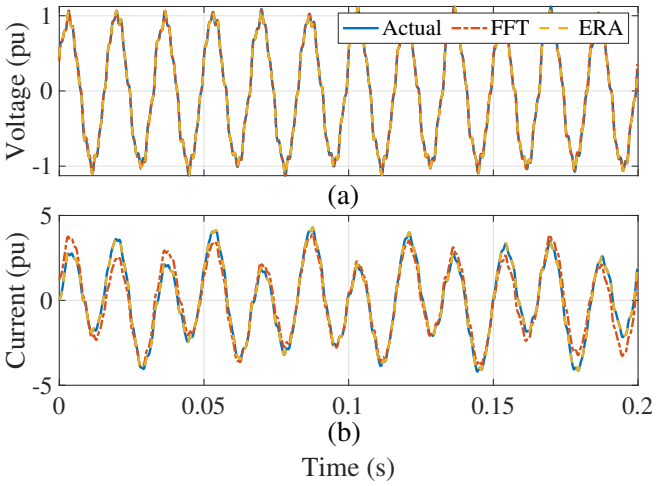

Fig. 18. Reconstruction capacity of voltage and current waveforms taken at bus 2 through the FFT and ERA-based time-frequency methods.

TABLE VIII
SNR, SSE, MSE, AND RMSE ERRORS FOR VOLTAGE SIGNAL

Error	**ERA-based filter**	**FFT**
SNR	31.7869 dB	30.0047 dB
SSE	0.0064 V^2	1.0441 V^2
MSE	0.0000 V^2	0.0005 V^2
$RMSE$	0.0017 V	0.0213 V

TABLE IX
SNR, SSE, MSE, AND RMSE ERRORS FOR CURRENT SIGNAL

Error	**ERA-based filter**	**FFT**
SNR	31.2063 dB	11.7699 dB
SSE	0.2723 A^2	755.6474 A^2
MSE	0.0001 A^2	0.3280 A^2
$RMSE$	0.0109 A	0.5727 A

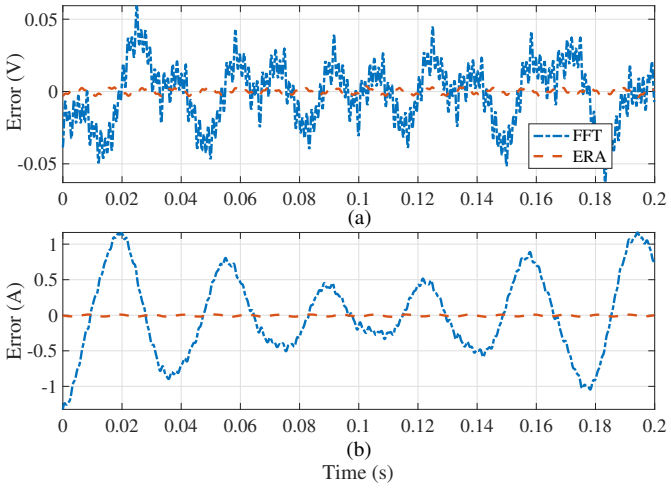

Fig. 19. Reconstruction errors for voltage and current signal at bus 2 of the Kundur power system.

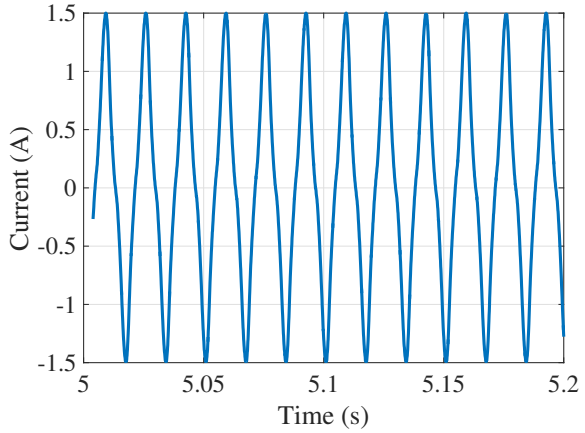

Fig. 20. Current waveform after the transformer energizing.

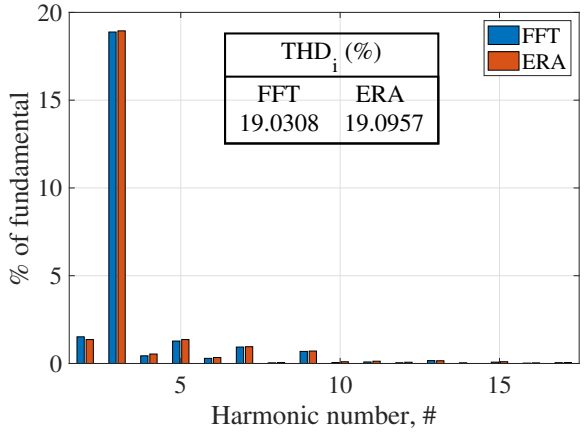

Fig. 21. Results of harmonic analysis processing current signals captured after transformer energizing.

form using the ERA and FFT methods. Notice that the current total harmonic distortion (THD_i) is about 19% for both methods. On the other hand, the frequency response of the ERA filters is illustrated in Fig. 22, where the filters extract the mono-components of the real transient event.

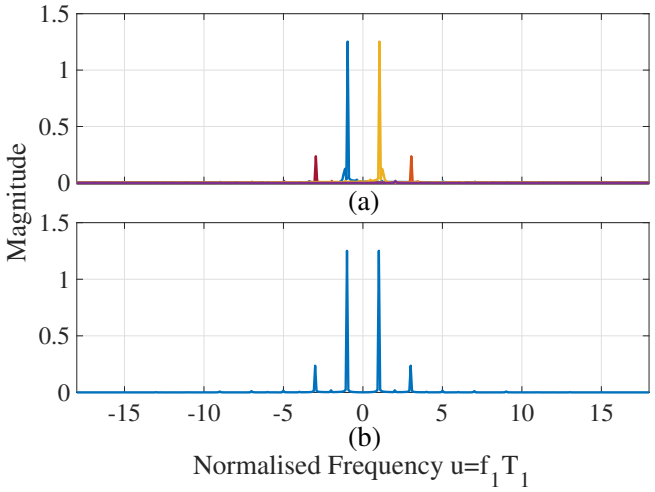

Fig. 22. Frequency responses for the real transient event. (a) ERA filters and (b) FFT filters.

TABLE X
SNR, SSE, MSE, AND RMSE ERRORS FOR REAL TRANSIENT EVENT

Error	**ERA-based filter**	**FFT**
SNR	32.9469 dB	28.4146 dB
SSE	145.2854 A^2	585.4849 A^2
MSE	0.0581 A^2	0.2345 A^2
$RMSE$	0.2412 A	0.4842 A

Furthermore, details of the harmonics (frequencies and amplitudes) are summarized in Table XI, where both methods showcase high similarity. To confirm the good performance of the proposed method, Fig. 23 shows the reconstructed signals using the estimated parameters for both methods, meanwhile the reconstruction capacity is also quantified by the SNR, SSE, MSE, and RMSE metrics depicted in Table X.

In this real event, the ERA-based harmonic estimates have the lowest error with 2.0075 times smaller than FFT. Besides, the reconstruction errors in Fig. 24 indicate that the approximation of the ERA filter bank provides the lowest error.

TABLE XI
RESULTS OF HARMONIC MONITORING THROUGH THE ERA-BASED AND FFT ANALYSES FOR A CURRENT SIGNAL RESULTING AFTER TRANSFORMER ENERGIZING

Harm. order	Frequency (Hz)		Amplitude (A)		Phase (degrees)	
	FFT	ERA	FFT	ERA	FFT	ERA
1	60.0863	59.9711	1.2514	1.2522	-115.2566	-111.9891
2	120.1727	119.9597	0.0190	0.0171	-121.4676	-115.1614
3	180.2591	179.9128	0.2363	0.2373	8.2559	18.4394
4	240.3455	239.8982	0.0055	0.0067	159.2478	167.9212
5	300.4319	299.8471	0.0160	0.0171	90.1197	108.4015
6	360.5183	359.8907	0.0037	0.0042	-173.7074	-162.7228
7	420.6047	419.7774	0.0117	0.0120	167.0460	-170.5386
8	480.6911	479.7218	0.0005	0.0007	-131.8041	-126.6971
9	540.7775	539.7579	0.0086	0.0089	-153.1151	-126.3432
10	600.8638	599.8648	0.0007	0.0012	11.1870	61.0190
11	660.9502	659.2298	0.0011	0.0016	110.3582	153.5182
12	721.0366	719.7051	0.0005	0.0009	23.8827	79.9579
13	781.1230	779.7034	0.0021	0.0020	-31.9318	14.0985
14	841.2094	–	0.0005	–	-87.5026	–
15	901.2958	899.2386	0.0010	0.0013	-28.3179	39.7488
16	961.3822	964.1981	0.0003	0.0004	-158.6426	4.0336
17	1021.4686	1020.5256	0.0006	0.0007	99.5365	117.8914

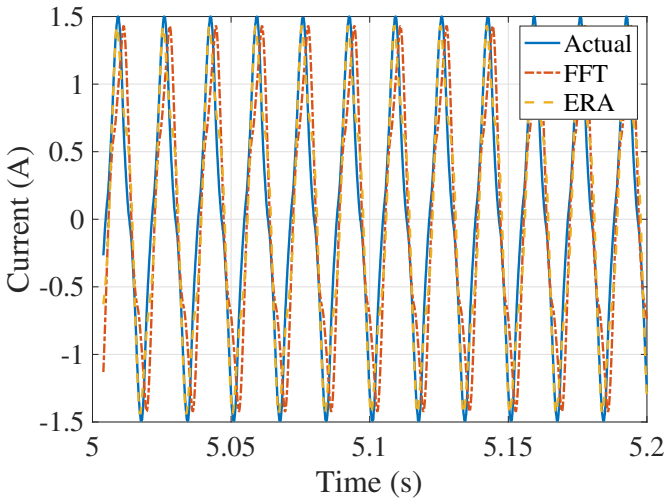

Fig. 23. Reconstruction capacity of the FFT and ERA for a real transient event.

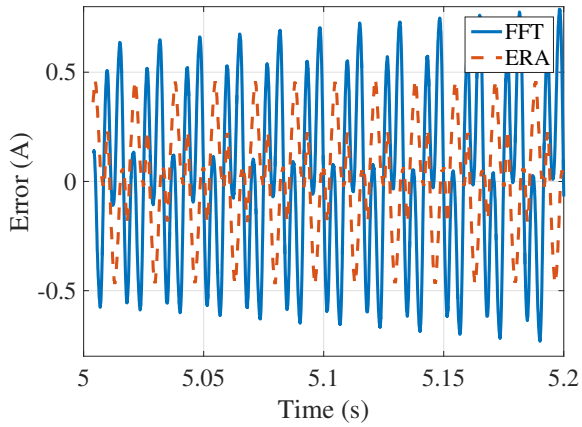

Fig. 24. FFT and ERA reconstruction errors for a real transient event.

IV. Conclusions

This paper demonstrates the ERA-based filter capacity to perform harmonic monitoring in power quality when harmonics are present in the power grid. The key idea behind our proposal lies in estimating all harmonic, inter-harmonic, and sub-harmonic components via a system identification technique that can render estimates such as harmonic amplitude and harmonic frequency even under high distortion conditions.

Our proposal was tested using simulated and real signals captured from simulated and real data. Thanks to its ability to provide new features, such as frequency identification without prior knowledge of frequency, as in the case of the FFT method, it is helpful to identify and monitor harmonics in power systems, making our proposal a robust and reliable tool for harmonic monitoring systems.

Acknowledgments

M.R.A. Paternina acknowledges financial support from the Project Support Program for Research and Technological Innovation of UNAM (DGAPA, PAPIIT-2023-2025) through the project IT102723. Also, authors from the Universidad Michoacana acknowledge the support provided by CONAHCYT through Project CF-2023-I-1174 within the framework of the "Ciencia de Frontera 2023".

References

[1] L. Qi, L. Qian, S. Woodruff, and D. Cartes, "Prony analysis for power system transient harmonics," *EURASIP Journal on Advances in Signal Processing*, vol. 2007, no. 1, p. 048406, 2007. doi: 10.1155/2007/48406.

[2] I. Kamwa, ed., *Monitoring and Control using Synchrophasors in Power Systems with Renewables*. Energy Engineering, Institution of Engineering and Technology, 2020.

[3] S. A. Soliman and A. M. Alkandari, "Electric power systems harmonics - identification and measurements," in *Power Quality* (G. R. Rey and L. M. Muneta, eds.), ch. 1, Rijeka: IntechOpen, 2011. doi: 10.5772/16412.

[4] A. Alizade and J. B. Noshahr, "Evaluating noise and dc offset due to inter-harmonics and supra-harmonics caused by back-to-back converter of (dfig) in ac distribution network," *CIRED*, vol. 2017, pp. 629–632, 2017. doi: 10.1049/oap-cired.2017.0045.

[5] A. E. Arranz Gimón, A. Zorita, D. Morí ñigo Sotelo, and O. Duque, "A review of total harmonic distortion factors for the measurement of harmonic and interharmonic pollution in modern power systems," *Energies*, vol. 14, p. 6467, 10 2021. doi: https://doi.org/10.3390/en14206467.

[6] P. F. Ribeiro, C. A. Duque, P. M. Ribeiro, and A. S. Cerqueira, *Power Systems Signal Processing for Smart Grids*. Wiley, 2014. doi: 10.1002/9781118639283.

[7] S. Ghosh and D. Chatterjee, "Non-intrusive identification of harmonic polluting loads in a smart residential system," *Sustainable Energy, Grids and Networks*, vol. 26, p. 100446, 2021. doi: https://doi.org/10.1016/j.segan.2021.100446.

[8] V. Ravindran, S. K. Rönnberg, and M. H. Bollen, "Interharmonics in pv systems: a review of analysis and estimation methods; considerations for selection of an apt method," *IET Renewable Power Generation*, vol. 13, no. 12, pp. 2023–2032, 2019. doi: https://doi.org/10.1049/iet-rpg.2018.5697.

[9] A. Andreotti, A. Bracale, P. Caramia, and G. Carpinelli, "Adaptive prony method for the calculation of power-quality indices in the presence of nonstationary disturbance waveforms," *IEEE Transactions on Power Delivery*, vol. 24, no. 2, pp. 874–883, 2009. doi: 10.1109/TPWRD.2008.923992.

[10] I. Y.-H. Gu and M. H. J. Bollen, "Estimating interharmonics by using sliding-window esprit," *IEEE Trans. Power Deliv.*, vol. 23, no. 1, pp. 13–23, 2008. doi: 10.1109/TPWRD.2007.911130.

[11] J.-Q. Lin, S.-C. Chan, and H.-C. Wu, "A robust past-based esprit algorithm with variable forgetting factor and regularization for frequencies/harmonics estimation in impulsive noise," *IEEE Transactions on Instrumentation and Measurement*, vol. 71, pp. 1–13, 2022. doi: 10.1109/TIM.2022.3173613.

[12] H. C. Lin, "Development of interharmonics identification using enhanced-fft algorithm," *The Journal of Engineering*, vol. 2017, no. 7, pp. 333–342, 2017. doi: https://doi.org/10.1049/joe.2017.0133.

[13] C. Altintasi, O. Aydin, M. C. Taplamacioglu, and O. Salor, "Power system harmonic and interharmonic estimation using vortex search algorithm," *Electric Power Systems Research*, vol. 182, p. 106187, 2020. doi: https://doi.org/10.1016/j.epsr.2019.106187.

[14] R. A. de Oliveira, V. Ravindran, S. K. Rönnberg, and M. H. Bollen, "Deep learning method with manual post-processing for identification of spectral patterns of waveform distortion in pv installations," *IEEE Transactions on Smart Grid*, vol. 12, no. 6, pp. 5444–5456, 2021. doi: 10.1109/TSG.2021.3107908.

[15] C. Ge, R. A. Oliveira, I. Y. Gu, and M. H. Bollen, "Unsupervised deep learning and analysis of harmonic variation patterns using big data from multiple locations," *Electric Power Systems Research*, vol. 194, p. 107042, 2021. doi: https://doi.org/10.1016/j.epsr.2021.107042.

[16] A. Eslami, M. Negnevitsky, E. Franklin, and S. Lyden, "Review of ai applications in harmonic analysis in power systems," *Renewable and Sustainable Energy Reviews*, vol. 154, p. 111897, 2022. doi: https://doi.org/10.1016/j.rser.2021.111897.

[17] K. Sheshyekani, G. Fallahi, M. Hamzeh, and M. Kheradmandi, "A general noise-resilient technique based on the matrix pencil method for the assessment of harmonics and interharmonics in power systems," *IEEE Transactions on Power Delivery*, vol. 32, no. 5, pp. 2179–2188, 2017. doi: 10.1109/TPWRD.2016.2625329.

[18] Y. E. Vatankulu, Z. Şentürk, and O. Salor, "Harmonics and interharmonics analysis of electrical arc furnaces based on spectral model optimization with high-resolution windowing," *IEEE Transactions on Industry Applications*, vol. 53, no. 3, pp. 2587–2595, 2017. doi: 10.1109/TIA.2017.2669328.

[19] Z. Jin, H. Zhang, F. Shi, Y. Sun, and V. Terzija, "A robust and adaptive detection scheme for interharmonics in active distribution network," *IEEE Transactions on Power Delivery*, vol. 33, no. 5, pp. 2524–2534, 2018. doi: 10.1109/TPWRD.2018.2815565.

[20] T. Lobos, T. Kozina, and H.-J. Koglin, "Power system harmonics estimation using linear least squares method and svd," in *IMTC/99. Proceedings of the 16th IEEE Instrumentation and Measurement Technology Conference (Cat. No.99CH36309)*, vol. 2, pp. 789–794 vol.2, 1999. doi: 10.1109/IMTC.1999.776975.

[21] N. Köse, Özgül Salor, and K. Leblebicioğlu, "Interharmonics analysis of power signals with fundamental frequency deviation using kalman filtering," *Electric Power Systems Research*, vol. 80, no. 9, pp. 1145–1153, 2010. doi: https://doi.org/10.1016/j.epsr.2010.03.006.

[22] J. Sanchez-Gasca and D. Trudnowski, "Identification of electromechanical modes in power system," tech. rep., IEEE Task Force on Identification of Electromechanical Modes of the Power System Stability, Power & Energy Society, June 2012. doi: 10.17023/2nn1-tn85.

[23] J.-N. Juang and R. S. Pappa, "An eigensystem realization algorithm for modal parameter identification and model reduction," *Journal of Guidance, Control, and Dynamics*, vol. 8, no. 5, pp. 620–627, 1985. doi: https://doi.org/10.2514/3.20031.

[24] J. A. de la O Serna, G. Castillo-García, M. R. Arrieta-Paternina, and A. Zamora-Méndez, "8 - power quality harmonic monitoring by the o-splines-based multiresolution signal decomposition," in *Monitoring and Control of Electrical Power Systems Using Machine Learning Techniques* (E. Barocio Espejo, F. R. Segundo Sevilla, and P. Korba, eds.), pp. 191–217, Elsevier, 2023. doi: https://doi.org/10.1016/B978-0-32-399904-5.00014-4.

[25] "Electromagnetic compatibility (emc) - part 4-7: Testing and measurement techniques - general guide on harmonics and interharmonics measurement and instrumentation, for power supply systems and equipment connected thereto," *IEC 61000-4-7:2002+AMD1:2008 CSV 2008*.

[26] S. I. Inc., "Sas/stat® 15.1 user's guide. cary, nc: Sas institute inc.." https://documentation.sas.com/doc/en/helpcenterwlcm/1.0/home.htm, 2018.

[27] M. R. A. Paternina, J. M. Ramirez-Arredondo, J. D. Lara-Jimenez, and A. Zamora-Mendez, "Dynamic equivalents by modal decomposition of tie-line active power flows," *IEEE Transactions on Power Systems*, vol. 32, pp. 1304–1314, March 2017. doi: 10.1109/TPWRS.2016.2572601.

[28] A. Zamora-Mendez, F. Zelaya-A, J. A. de la O Serna, J. H. Chow, and M. R. A. Paternina, "Model-based synchrophasor estimation by exploiting the eigensystem realization approach," *Electric Power Systems Research*, vol. 182, p. 106249, 2020. doi: https://doi.org/10.1016/j.epsr.2020.106249.

[29] International Business Machines Corp.,, Hopewell Junction, NY., *IBM (2008, Jan). PowerPC 970MP RISC Microprocessor. Version 1.3.*

[30] S. Documentation, "Harmonic analysis of a three-phase rectifier." https://www.mathworks.com/help/sps/ug/harmonic-analysis-of-a-three-phase-rectifier.html, 2020.

[31] K. Sakai, "Power quality analyzer pq3100." Available here, HIOKI E.E. CORPORATION. Vol. 3, 2017, No. 1. Technical Notes.

[32] P. Kundur, *Power system stability and control*. McGraw-hill, Inc., New York, 1994.

[33] V. Preciado, M. Madrigal, E. Muljadi, and V. Gevorgian, "Harmonics in a wind power plant," in *2015 IEEE Power & Energy Society General Meeting*, pp. 1–5, 2015. doi: https://doi.org/10.1109/PESGM.2015.7285774.

[34] M. B. Marz, "Interharmonics : What they are , where they come from and what they." Available here, American Transmission Company, Waukesha, WI, 2016. Power Quality Blog.

[35] P. Gnaciński, D. Hallmann, P. Klimczak, A. Muc, and M. Pepliński, "Effects of negative sequence voltage subharmonics on cage induction motors," *Energies*, vol. 15, no. 23, 2022. doi: 10.3390/en15238797.

[36] Z. Wen, S. Peng, J. Yang, J. Deng, H. He, and T. Wang, "Analysis of the propagation characteristic of subsynchronous oscillation in wind integrated power system," *Energies*, vol. 12, no. 6, 2019. doi: 10.3390/en12061081.

Miguel G. Juarez obtained his B.S. and M.Sc. degrees in electrical engineering from Universidad Michoacana de San Nicolas de Hidalgo (UMSNH), Morelia, Michoacan in 2021 and 2024, respectively.

Félix Reyes-Maldonado obtained his B.S. degree in electrical engineering from Universidad Michoacana de San Nicolas de Hidalgo (UMSNH), Morelia, Michoacan in 2021. He is currently working toward an M.Sc. degree in electrical engineering at UMSNH.

Alejandro Zamora-Méndez (M' 11) obtained his B.S. and M.Sc. in Electrical Engineering from Universidad Michoacana de San Nicolas de Hidalgo (UMSNH), Morelia, Mexico, in 2005 and 2008, respectively. He joined the Electrical Engineering Faculty, UMSNH in 2008. He received a D.Sc. degree in Electrical Engineering from CINVESTAV-Guadalajara in 2016.

José Ortiz-Bejar received the Ph.D. degree in data science from INFOTEC, Unidad Aguascalientes, in 2020. He is currently an associate professor with the Michoacan University of San Nicolás de Hidalgo. He has served as an Organizer of ROPEC and IEEE T&DLA conferences. His research interest centers on machine learning applied to power systems analysis, text categorization, and clustering.

Juan Carlos Silva Chavez (Member, IEEE) received the Bachelor of Engineering degree in electrical engineering and the Master of Science from Instituto Tecnologico de Morelia, Morelia, Michoacan, Mexico in 1998 and 2001 respectively, and Doctor of Engineering degrees in electrical engineering from the Universidad Michoacana de San Nicolas de Hidalgo, Morelia, Michoacan, Mexico, in 2006. He is currently working as a faculty member at Universidad Michoacana de San Nicolas de Hidalgo, Morelia, Michoacan. His research interests include power system restructuring, power system planning, smart grid technologies, meta-heuristic optimization techniques, reliability analysis of renewable energy systems, power quality analysis, renewable energy integration, and electricity market.

Mario R. Arrieta Paternina (M' 11) holds a B.Eng. and M.Eng. in Electrical Engineering from National University of Colombia, Medellin, Colombia, in 2007 and 2009, respectively. In 2017, he obtained his D.Sc. degree in Electrical Engineering from CINVESTAV, and joined the Department of Electrical Engineering at the UNAM.

V. Torres-García (Senior, IEEE) received his M.Sc. and D.Sc. degrees in Electrical Engineering from the Instituto Tecnológico de Morelia, in 2009 and 2015, respectively. He is currently with the PGIIE of the TecNM campus Morelia. His research interest areas include electric power systems, distribution networks, harmonics, electromagnetic transients, and power systems protections.